

Surface regeneration of sulfur-poisoned Ni surfaces under SOFC operation conditions predicted by first-principles-based thermodynamic calculations

Jeng-Han Wang, MeiLin Liu *

School of Materials Sciences and Engineering, Georgia Institute of Technology, Atlanta, GA 30332, USA

Received 7 September 2007; received in revised form 9 October 2007; accepted 9 October 2007

Available online 18 October 2007

Abstract

The surface regeneration or de-sulfurization process of a sulfur-poisoned (i.e. sulfur-covered) nickel surface by O_2 and H_2O has been studied using first-principles calculations with proper thermodynamic corrections. While O_2 is more effective than H_2O in removing the sulfur atoms adsorbed on nickel surface, it readily reacts with the regenerated Ni surface, leading to over-oxidization of Ni. Thus, H_2O appears to be a better choice for the surface regeneration process. In reality, however, both O_2 and H_2O may be present under fuel cell operating conditions. Accordingly, the effects of the partial pressures of O_2 [p_{O_2}] and H_2O [p_{H_2O}] as well as the ratio of p_{O_2}/p_{H_2O} on the regeneration of a sulfur-covered Ni surface without over-oxidization at different temperatures are systematically examined to identify the best conditions for regeneration of Ni-based SOFC anodes under practical conditions.

© 2007 Elsevier B.V. All rights reserved.

Keywords: Solid oxide fuel cell; Sulfur poisoning; Surface regeneration; Thermodynamics corrected first-principle calculations; Phase diagram

1. Introduction

Sulfur-containing compounds are the most commonly encountered contaminants in readily available fuels and are difficult to be completely removed efficiently and economically. Even with small amount, they severely degrade the performance of catalysts for fuel reforming or the anodes in solid oxide fuel cells (SOFC). The poisoning effect or the degradation in performance is generally believed due to the adsorption of sulfur on the surface of catalysts or SOFC anodes, which blocks the active sites for desirable reactions [1]. Thus, the removal of the atomically adsorbed sulfur from surfaces is a critical step toward sulfur tolerance.

To date, the de-sulfurization of various materials has been extensively studied via experimental and computational approaches, including pure metals (Ni [2–4], Cu [5], Mo [6,7] and Pt [8,9]) as electrodes, small clusters (CoMo, NiMo [7,10], Ni_2P , Mo_2C [11], MoS_2 [12,13]) as catalysts, and metal oxides (CeO_2 [14–16], ZrO_2 [17,18] and La_2O_3 [19]) as electrolytes in fuel cells. It is well known that the good overlaps between sulfur p orbital and transition metal d orbitals result in strong S-metal bond formation, making the de-sulfurization process difficult. Small clusters of several metals display better properties for de-sulfurization. This enhancement is attributed to the *promoting effect* in CoMo and NiMo cases [7,10] and to the stabilization of nickel d orbital in the Ni_2P case [11]. Among the metal oxide compounds, a highly reactive oxide of La_2O_3 was found to be an promising material to efficiently remove H_2S contaminant from fuels due to the dual valance charges of La^{III} and La^{IV} [19].

Furthermore, various chemical reagents have been thoroughly studied in the regeneration process, including H_2 [20–22], O_2 [2,4,16] and H_2O [15,23,24]. The surface de-sulfurization by H_2 forming H_2S , which is the reversed reaction of the highly exothermic sulfuration process, $H_2S \rightarrow S(a) + H_2$ [9,25–28], has shown to be less efficient. On the other hand, the oxidation of sulfur by O_2 and H_2O to form SO_2 shows more promising results. However, over dosing these reagents on metal surfaces results in metal

* Corresponding author. Tel.: +1 404 894 6114; fax: +1 404 894 9140.
E-mail address: meilin.liu@mse.gatech.edu (M. Liu).

oxide formation and degrades the catalytic activity of Ni-based catalysts. Thus, determining the right conditions to de-sulfurize a sulfur-poisoned surface without over dosing is a critical issue to achieve surface regeneration.

Here we report the results on our systematic examination of proper conditions for regeneration of sulfur-poisoned Ni surfaces. In this analysis, we used DFT to compute the heat of reactions and thermodynamic corrections to estimate the Gibbs free energies of the interfacial reactions, producing phase diagrams important to the de-sulfurization processes of Ni surface. The over-oxidation of Ni surfaces by excess reagents is also considered. Further, proper conditions for the use of O₂, H₂O, and a mixture of them for de-sulfurization without over-oxidation have also been studied.

2. Computational method

The adsorption of atomic S(a) on Ni surfaces and bulk phases of pure Ni and NiO are computed by Vienna Ab Initio Simulation Package (VASP) [29–31], implementing the density functional theory (DFT). The exchange–correlation function treated by the generalized gradient approximation with the Perdew–Burke–Ernzerhof formulation, known as GGA-PBE [32,33], is applied for the total energy calculations. Combining the accuracy of augmented plane waves with the cost-effective pseudopotentials implemented in VASP, the projector-augmented wave method (PAW) [34,35] is applied in the basis set. The kinetic cut-off energy of 400 eV is employed to ensure the convergence with respect to the basis set and the efficiency of the computational cost. The Brillouin-zone (BZ) integration is sampled with $0.05 \text{ \AA}^{-1} \times 2 \text{ \AA}^{-1}$ spacing in reciprocal space by Monkhorst–Pack scheme [36]. All calculations are performed imposing zero magnetization.

In poly-crystalline Ni catalysts or electrodes, Ni(1 0 0) surface forms the most stable S(a) adsorption and is considered as the most vulnerable surface orientation to be poisoned under SOFC operation conditions [37]. Thus, the (1 0 0) surface is applied in the current calculations. Although sulfur may adsorb on surfaces of other orientations, it is easier to remove sulfur from these surfaces than from the (1 0 0) surface. The Ni bulk is initially computed to predict the theoretical lattice parameter. The result shows that the computed lattice constant of 3.58 \AA is in good agreement with the experimental value of 3.52 \AA [38], and employed for the surface calculations. The surface is modeled by the super cells of four-layer Ni(1 0 0) slab with 64 Ni atoms, as shown in Fig. 1, followed by a 10- \AA vacuum space. The S(a) adsorption energies have been initially computed to test the convergence. The result show that the surface models with 5 and 6 Ni(1 0 0) slabs or larger vacuum space, 15 \AA , have similar adsorption energies, less than 0.01-eV difference, to the applied surface model, four-layer Ni(1 0 0) slab and 10- \AA vacuum space. The Monkhorst–Pack *k*-points are set as $2 \times 2 \times 1$ along $(1\ 1\ 0) \times (1\bar{1}\ 0) \times (0\ 0\ 1)$ directions. The modeled surface with the area of $9.90 \text{ \AA} \times 9.90 \text{ \AA}$ and 16 fourfold hollow sites (the most stable adsorption sites) is large enough to avoid any adsorbate–adsorbate interaction and to simulate minimum coverage of S(a) with the highest adsorption energies. The top three layers are relaxed and the bottom one layer is fixed at the computed lattice constant to represent the semi-infinite bulk crystal beneath the surface during the calculation.

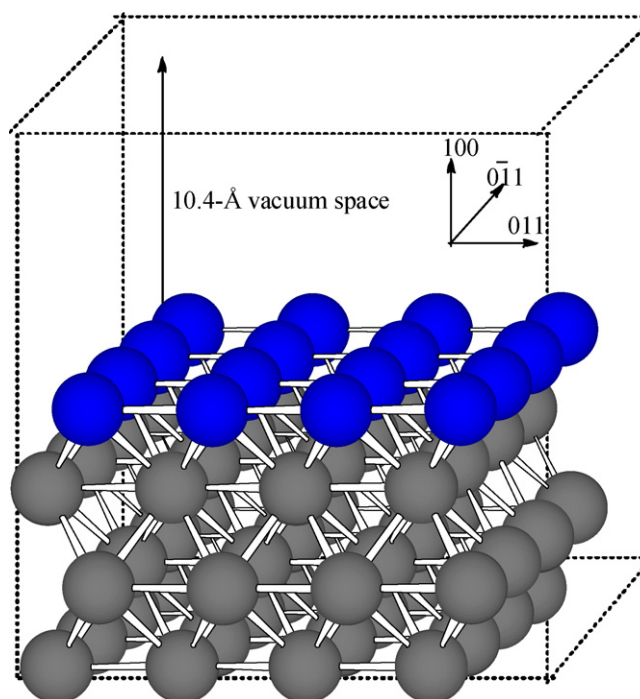


Fig. 1. The Ni(1 0 0) surface is constructed by 64 Ni atoms with a 10.4- \AA vacuum space. The blue balls are the surface Ni atoms. The dash lines represent the volume of the super cell. (For interpretation of the references to color in this figure legend, the reader is referred to the web version of the article.)

Considering the effect of temperature and partial pressure of various gases, we calculated the Gibbs free energy $G(T, p)$ of the whole system by applying the thermodynamic corrections on the DFT computed energy, E^{DFT} , which represents the Gibbs free energy at 0 K in vacuum or the Helmholtz free energy, $F(T)$, at 0 K, $E^{\text{DFT}} = G(0, 0) = F(0)$.

For a general gas–surface reaction:



where surface1 and surface2 represent the reactant and product, respectively, in the condense phase whereas gas1(g) and gas2(g) correspond to the reactant and product, respectively, in the gas phase. The Gibbs free energy for reaction (1) can be expressed as

$$\Delta G(T, p) = (G_{\text{gas2}} + G_{\text{surface2}}) - (G_{\text{gas1}} + G_{\text{surface1}}) \quad (2)$$

It has been proven [39,40] that the Gibbs free energies of surfaces have relatively small variation, <10 meV, in a wide range of temperature (<1500 K) and pressure (<100 atm) and the vibrational and entropic contributions to Gibbs free energies of atomic adsorbates are negligible. Therefore, the Gibbs free energies of solid phases can be approximated by the internal energy computed from DFT calculations, $G_{\text{surface}}(T, p) \approx G_{\text{surface}}(0, 0) = E_{\text{surface}}^{\text{DFT}}$. In contrast, the Gibbs free energies of the gas phases are strongly affected by the temperatures and pressures and can be expressed as

$$G_{\text{gas}}(T, p) = G_{\text{gas}}(0, 0) + \Delta G_{\text{gas}}(0 \rightarrow T, p^0) + \Delta G_{\text{gas}}(T, p^0 \rightarrow p) = E_{\text{gas}}^{\text{DFT}} + H_{\text{gas}}(T, p^0) + RT \ln(p_{\text{gas}}/p^0) \quad (3)$$

The first term is directly from DFT calculations. The second term, which can be found in the empirical thermodynamic database [41], is the standard enthalpies of the gas phase molecules contributing from rotations, vibrations, and ideal-gas entropy at p^0 and is temperature-dependent. The third term is a partial pressure-dependent function from Maxwell relation (where R is the gas constant). Therefore, at a given pressure and temperature, the Gibbs free energy can be obtained by adding the thermodynamic corrections in the last two terms to the DFT results, as discussed previously [12,42,43], and the Gibbs free energy for reaction (1) can be re-written as

$$\begin{aligned} \Delta G(T, p) &= (E_{\text{surface2}}^{\text{DFT}} - E_{\text{surface1}}^{\text{DFT}}) + (E_{\text{gas2}}^{\text{DFT}} - E_{\text{gas1}}^{\text{DFT}}) + (H_{\text{gas2}} - H_{\text{gas1}}) + RT (\ln [p_{\text{gas2}}] - \ln [p_{\text{gas1}}]) \\ &= \Delta E^{\text{DFT}}(0, 0) + \Delta H(T, p^0) + RT \ln \left[\frac{p_{\text{gas2}}}{p_{\text{gas1}}} \right] \end{aligned} \quad (4)$$

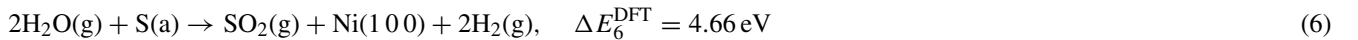
The feasibility of the gas–surface reactions can be determined from the computed $\Delta G(T, p)$, as a function of ΔE^{DFT} , enthalpy, temperature and pressure.

The thermodynamic correction of external electric field is excluded in the current calculations since the external electric field, which exists in the electrochemical reactions under SOFC operation conditions, has relatively smaller contribution in the Gibbs free energy calculations, as examined in the Ni–S system [37].

3. Results and discussion

3.1. Regeneration by O_2 or H_2O

The sulfur poisoning effect of anode for an SOFC is resulted from the atomic sulfur adsorbed on the Ni surface, which blocks the active sites for fuel oxidation [1,37]. To regenerate the surface, therefore, the adsorbed atomic sulfur must be removed from the surfaces by introducing oxidizing reagents to react with the adspecies. The de-sulfurization process using the oxidant reagents of O_2 and H_2O can be described as follows:



where ΔE_5^{DFT} and ΔE_6^{DFT} are the heat of reactions (5) and (6), respectively, which can be determined from DFT calculations.

$$\Delta E_5^{\text{DFT}} = (E_{\text{SO}_2}^{\text{DFT}} + E_{\text{Ni}(100)}^{\text{DFT}}) - E_{\text{O}_2}^{\text{DFT}} + E_{\text{S}(a)}^{\text{DFT}} \quad (7)$$

$$\Delta E_6^{\text{DFT}} = (E_{\text{SO}_2}^{\text{DFT}} + E_{\text{Ni}(100)}^{\text{DFT}} + 2E_{\text{H}_2}^{\text{DFT}}) - (2E_{\text{H}_2\text{O}}^{\text{DFT}} + E_{\text{S}(a)}^{\text{DFT}}) \quad (8)$$

As described in the S–Ni system, the most stable S(a) adsorbed on the fourfold hollow site of Ni(100) surface with the lowest surface coverage [37] considered as the decisive poison species, is applied in the present calculation. Since the non-adsorbed species are in the gas phase in the computed temperature range, 500–1600 K, the Gibbs free energies for reactions (5) and (6) are given by,

$$\Delta G_5 = (G_{\text{SO}_2} + G_{\text{Ni}(100)}) - (G_{\text{O}_2} + G_{\text{S}(a)}) = \Delta E_5^{\text{DFT}}(0, 0) + \Delta H_5(T, p^0) - RT \ln \left[\frac{p_{\text{O}_2}}{p_{\text{SO}_2}} \right] \quad (9)$$

$$\Delta G_6 = (G_{\text{SO}_2} + G_{\text{Ni}(100)} + 2G_{\text{H}_2}) - (2G_{\text{H}_2\text{O}} + G_{\text{S(a)}}) = \Delta E_6^{\text{DFT}}(0, 0) + \Delta H_6(T, p^0) - 2RT \ln \left[\frac{p_{\text{H}_2\text{O}}}{p_{\text{H}_2} p_{\text{SO}_2}^{0.5}} \right] \quad (10)$$

where $\Delta H_5(T, p^0)$ and $\Delta H_6(T, p^0)$ are the standard enthalpies of the gas phase species involved in reactions (5) and (6), respectively.

$$\Delta H_5(T, p^0) = H_{\text{SO}_2}(T, p^0) - H_{\text{O}_2}(T, p^0) \quad (11)$$

$$\Delta H_6(T, p^0) = H_{\text{SO}_2}(T, p^0) + 2H_{\text{H}_2}(T, p^0) - 2H_{\text{H}_2\text{O}}(T, p^0) \quad (12)$$

By computing the Gibbs free energies of ΔG_5 and ΔG_6 , as functions of temperature and pressures of p_{SO_2} , p_{O_2} , p_{H_2} and $p_{\text{H}_2\text{O}}$, the required de-sulfurization condition can be expressed in the thermodynamic diagrams in Fig. 2. The yellow regions represent the poisoned phase of S(a) adsorption and white regions represent the phase of clean Ni surface, regenerated by O_2 or H_2O . The boundaries between the yellow and the white regions correspond to $\Delta G_5 = 0$ in Eq. (9) and $\Delta G_6 = 0$ in Eq. (10).

$$\log \left[\frac{p_{\text{O}_2}}{p_{\text{SO}_2}} \right] = 0.434 \left[\frac{\Delta E_5^{\text{DFT}} + \Delta H_5}{RT} \right] = 0.434 \left[\frac{(E_{\text{SO}_2}^{\text{DFT}} + E_{\text{Ni}(100)}^{\text{DFT}}) - (E_{\text{O}_2}^{\text{DFT}} + E_{\text{S(a)}}^{\text{DFT}}) + (H_{\text{SO}_2} - H_{\text{O}_2})}{RT} \right] \quad (13)$$

$$\begin{aligned} \log \left[\frac{p_{\text{H}_2\text{O}}}{p_{\text{H}_2} p_{\text{SO}_2}^{0.5}} \right] &= 0.434 \left[\frac{\Delta E_6^{\text{DFT}} + \Delta H_6}{2RT} \right] \\ &= 0.434 \left[\frac{(E_{\text{SO}_2}^{\text{DFT}} + E_{\text{Ni}(100)}^{\text{DFT}} + 2E_{\text{H}_2}^{\text{DFT}}) - (2E_{\text{H}_2\text{O}}^{\text{DFT}} + E_{\text{S(a)}}^{\text{DFT}}) + H_{\text{SO}_2} + 2H_{\text{H}_2} - 2H_{\text{H}_2\text{O}}}{2RT} \right] \end{aligned} \quad (14)$$

For the O_2 case in Fig. 2(a), higher temperature requires more O_2 , or higher $\log [p_{\text{O}_2}/p_{\text{SO}_2}]$, to remove S(a) from the exothermic reaction (5). For H_2O case in Fig. 2(b), less H_2O , or lower $\log [p_{\text{H}_2\text{O}}/p_{\text{H}_2} p_{\text{SO}_2}^{0.5}]$, is needed at higher temperatures since the removal of S(a) by H_2O in reaction (6) has a high endothermicity.

It is noted that at higher or lower temperatures, the bulk nickel sulfide will be formed on the surface, as detailed in a previous study [37]. The boundaries between S(a) adsorption and nickel sulfide bulk are excluded since the S(a) adsorption is the most critical phase in the poisoning behavior; thus only the boundary between clean Ni surface and the S(a) adsorption phase is considered in the this analysis.

Considering the pressure effects at a given temperature, higher pressures of O_2 or H_2O can clean the S(a)-poisoned surface more efficiently; however, exposure to excess amount of O_2 or H_2O will over-oxidize the regenerated Ni, resulting in O(a) adsorption and NiO formation [2,4]. While O(a) adsorption can be readily removed by H_2 or other fuels, the formation of bulk NiO will significantly de-activate the Ni catalyst, due mostly to the volume change associated with the redox reaction of Ni. Taking this into consideration, we have to carefully examine the Ni–NiO bulk phase equilibrium in the O_2 –Ni and H_2O –Ni systems.

The reactions between Ni and O_2 or H_2O forming NiO can be expressed as

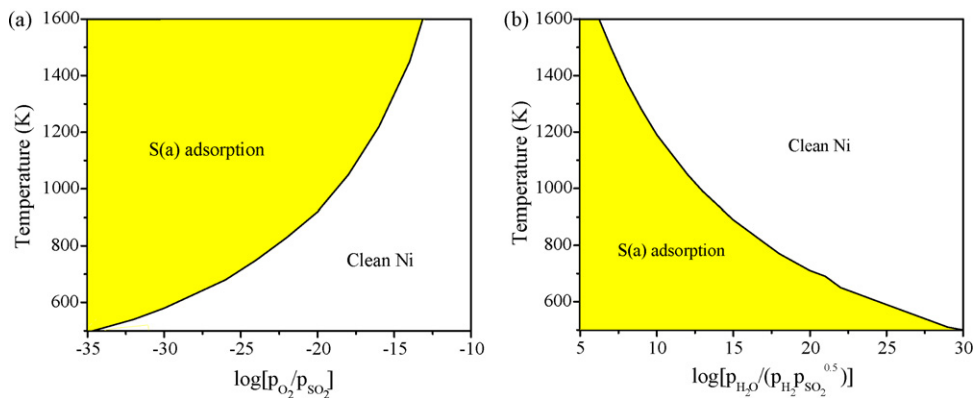


Fig. 2. The thermodynamic diagram for S(a) removal process by (a) O_2 and (b) H_2O in reactions (5) and (6), respectively. The yellow and white regions represent the poisoned S(a) adsorption and regenerated Ni surfaces, respectively. (For interpretation of the references to color in this figure legend, the reader is referred to the web version of the article.)

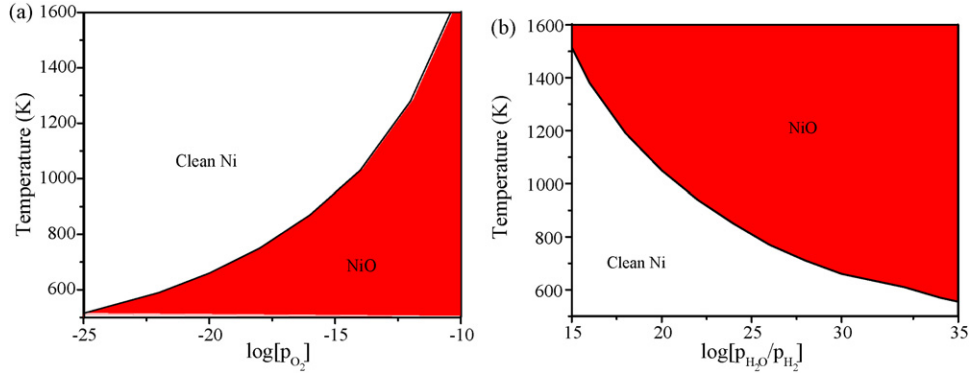


Fig. 3. The thermodynamic diagram for (a) O₂ and (b) H₂O interacting with Ni forming NiO. The white regions correspond to the phase of clean Ni. The red regions correspond to the phase of NiO bulk formation in reactions (15) and (16). (For interpretation of the references to color in this figure legend, the reader is referred to the web version of the article.)

Similarly, the corresponding Gibbs free energies for reactions (15) and (16) can be computed as

$$\Delta G_{15} = (E_{\text{NiO}}^{\text{DFT}} - E_{\text{Ni}}^{\text{DFT}}) - \frac{1}{2}(E_{\text{O}_2}^{\text{DFT}} + H_{\text{O}_2}(T, p^0) - RT \ln[p_{\text{O}_2}]) \quad (17)$$

$$\Delta G_{16} = E_{\text{NiO}}^{\text{DFT}} - E_{\text{Ni}}^{\text{DFT}} + E_{\text{H}_2}^{\text{DFT}} - E_{\text{H}_2\text{O}}^{\text{DFT}} + H_{\text{H}_2}(T, p^0) - H_{\text{H}_2\text{O}}(T, p^0) - RT \ln \left[\frac{p_{\text{H}_2\text{O}}}{p_{\text{H}_2}} \right] \quad (18)$$

Shown in Fig. 3 are the thermodynamic diagrams for the O₂–Ni and H₂O–Ni systems constructed by the Gibbs free energy calculations. The red regions represent the over-oxidized phase of NiO formation and white regions represent the phase of pure Ni. The boundaries between the red and the white regions in Fig. 3(a) and (b) correspond to $\Delta G_{15} = 0$ in Eq. (17), and $\Delta G_{16} = 0$ in Eq. (18).

$$\log[p_{\text{O}_2}] = 0.434 \left[\frac{2E_{\text{NiO}}^{\text{DFT}} - (E_{\text{O}_2}^{\text{DFT}} + 2E_{\text{Ni}}^{\text{DFT}}) - H_{\text{O}_2}}{RT} \right] \quad (19)$$

$$\log \left[\frac{p_{\text{H}_2\text{O}}}{p_{\text{H}_2}} \right] = 0.434 \left[\frac{E_{\text{NiO}}^{\text{DFT}} - E_{\text{Ni}}^{\text{DFT}} + E_{\text{H}_2}^{\text{DFT}} - E_{\text{H}_2\text{O}}^{\text{DFT}} + H_{\text{H}_2} - H_{\text{H}_2\text{O}}}{RT} \right] \quad (20)$$

Since the NiO formation from O₂ reacting with Ni are exothermic, the NiO phases appear in the lower temperature range at a given O₂ partial pressure in Fig. 3(a). In contrast, the NiO formation from H₂O reacting with Ni is endothermic. Accordingly, the NiO phases appear in the high temperature region at a given $\log[p_{\text{H}_2\text{O}}/p_{\text{H}_2}]$ in Fig. 3(b). For the pressure effect, the NiO phases appear in the region with high O₂ and H₂O partial pressures, larger values of $\log[p_{\text{O}_2}]$ and $\log[p_{\text{H}_2\text{O}}/p_{\text{H}_2}]$, respectively, at a given temperature.

Therefore, the proper condition to regenerate the surface without over-oxidization can be determined by combining Figs. 2 and 3, as summarized in Fig. 4. Insufficient oxidant reagents of O₂ and H₂O results the S(a) phase in the upper left and lower left yellow regions in Fig. 4(a) and (b), respectively. The over dosed reagents of O₂ and H₂O results NiO formation in the lower right and upper right red regions in Fig. 4(a) and (b), respectively. The appropriate conditions to regenerate the Ni surface are located in the center white regions.

Specifically, the partial pressure range of O₂ in the white (clean Ni) region is resulted from (19) to (13):

$$\Delta \log[p_{\text{O}_2}] = 0.434 \left[\frac{2E_{\text{NiO}}^{\text{DFT}} - 2E_{\text{Ni}}^{\text{DFT}} - E_{\text{SO}_2}^{\text{DFT}} - E_{\text{Ni}(1.00)}^{\text{DFT}} + E_{\text{S(a)}}^{\text{DFT}} + H_{\text{SO}_2}}{RT} \right] - \log[p_{\text{SO}_2}] \quad (21)$$

The partial pressure range of $[p_{\text{H}_2\text{O}}/p_{\text{H}_2}]$ in the white region is resulted from (20) to (14):

$$\Delta \log \left[\frac{p_{\text{H}_2\text{O}}}{p_{\text{H}_2}} \right] = 0.434 \left[\frac{2E_{\text{NiO}}^{\text{DFT}} - 2E_{\text{Ni}}^{\text{DFT}} - E_{\text{SO}_2}^{\text{DFT}} - E_{\text{Ni}(1.00)}^{\text{DFT}} + H_{\text{SO}_2}}{2RT} \right] - \frac{1}{2} \log[p_{\text{SO}_2}] \quad (22)$$

Therefore, the allowed ranges of $\Delta \log[p_{\text{O}_2}]$ and $\Delta \log[p_{\text{H}_2\text{O}}/p_{\text{H}_2}]$ for the O₂ and H₂O regenerations, respectively, depend strongly on the partial pressures of p_{SO_2} : the lower p_{SO_2} in the system will allow wider ranges of $\Delta \log[p_{\text{O}_2}]$ or $\Delta \log[p_{\text{H}_2\text{O}}/p_{\text{H}_2}]$. The partial pressures of p_{SO_2} produced from the O₂ in reaction (5) is expected to be higher than that produced from H₂O in reaction (6) since the stronger O₂ oxidant generates SO₂ faster and leave more residual SO₂. Therefore, the last terms in Eqs. (21) and (22) will further narrow the proper pressure range for O₂ but widen that for H₂O to achieve complete regeneration but without over oxidation

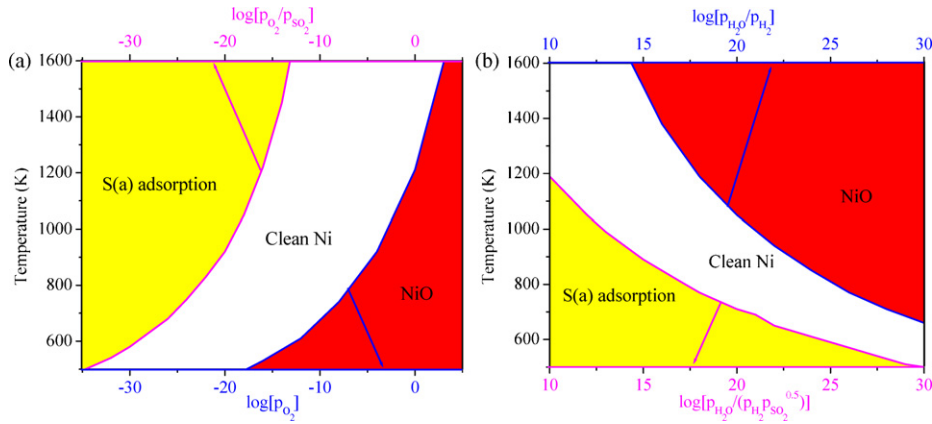
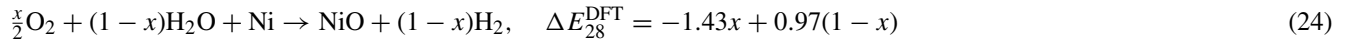
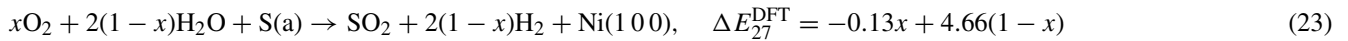


Fig. 4. The complete (T, p) diagram for (a) O_2 and (b) H_2O interacting with sulfur adsorbed Ni surface. The yellow, white, and red regions represent the phases of S(a) adsorption, clean Ni, and NiO bulk, respectively. The proper conditions for surface regeneration without oxide formation are located in the central white regions. The boundaries between yellow and white regions correspond to the axes of (a) $\log[p_{O_2}/p_{SO_2}]$ and (b) $\log[p_{H_2O}/p_{H_2}p_{SO_2}^{0.5}]$; the boundaries between white and red regions correspond to the axes of (a) $\log[p_{O_2}]$ and (b) $\log[p_{H_2O}/p_{H_2}]$, as arrowed. (For interpretation of the references to color in this figure legend, the reader is referred to the web version of the article.)

of Ni. In addition, the pressure range of O_2 is relatively difficult to be prepared in practical experiments. Thus, H_2O is considered as a better reagent for regeneration than O_2 as observed in the previous experiments [1,15,23].

3.2. Regeneration by a mixture of O_2 and H_2O

Under practical fuel cell operation conditions, both O_2 and H_2O may be present in the system. The surface de-sulfurization and over-oxidation can be described as follows:



where x varies from 0 to 1, depending on the ratio between O_2 and H_2O . At $x=0$, it is the pure H_2O regeneration process as described by reactions (6) and (16) while at $x=1$, it is the pure O_2 regeneration process in reactions (5) and (15).

The Gibbs free energies of reactions (23) and (24) can be expressed as

$$\Delta G_{23} = \Delta E_{23}^{DFT} + \Delta H_{23} + RT \ln \left[\frac{p_{SO_2} p_{H_2}^{2(1-x)}}{p_{O_2}^x p_{H_2O}^{2(1-x)}} \right] \quad (25)$$

$$\Delta G_{24} = \Delta E_{24}^{DFT} + \Delta H_{24} + RT \ln \left[\frac{p_{H_2}^{(1-x)}}{p_{O_2}^{x/2} p_{H_2O}^{(1-x)}} \right] \quad (26)$$

Where the internal energies and enthalpies are

$$\Delta E_{23}^{DFT} = 2(1-x)E_{H_2}^{DFT} + E_{SO_2}^{DFT} + E_{Ni(100)}^{DFT} - (xE_{O_2}^{DFT} + 2(1-x)E_{H_2O}^{DFT} + E_{S(a)}^{DFT}) \quad (27)$$

$$\Delta H_{23} = 2(1-x)H_{H_2} + H_{SO_2} - (xH_{O_2} + 2(1-x)H_{H_2O}) \quad (28)$$

$$\Delta E_{24}^{DFT} = (1-x)E_{H_2}^{DFT} + E_{NiO}^{DFT} - \left(\frac{x}{2}E_{O_2}^{DFT} + (1-x)E_{H_2O}^{DFT} + E_{Ni}^{DFT} \right) \quad (29)$$

$$\Delta H_{24} = (1-x)H_{H_2} - \left(\frac{x}{2}H_{O_2} + (1-x)H_{H_2O} \right) \quad (30)$$

From the Gibbs free energy calculation, the boundaries among the phases of clean Ni, S(a) and NiO from different values of x is shown in Fig. 5.

For the pressure effect, the required reagents to remove S(a) in reaction (23), $\log[p_{O_2}^{x/2} p_{H_2O}^{(1-x)} / p_{SO_2}^{0.5} p_{H_2}^{(1-x)}]$, and to form NiO in reaction (24), $\log[p_{O_2}^{x/2} p_{H_2O}^{(1-x)} / p_{H_2}^{(1-x)}]$, decrease as the x increases because less oxidants are needed in both cases as the component of stronger O_2 oxidant raises. For the temperature effect, reactions (23) and (24) are changed from exothermic to endothermic as x decreases since the pure O_2 regeneration ($x=1$) in reactions (5) and (15) are exothermic and the pure H_2O regeneration ($x=0$) in reactions (6) and (16) are endothermic. This result explains the boundary change, from left to right concave, as x decreases.

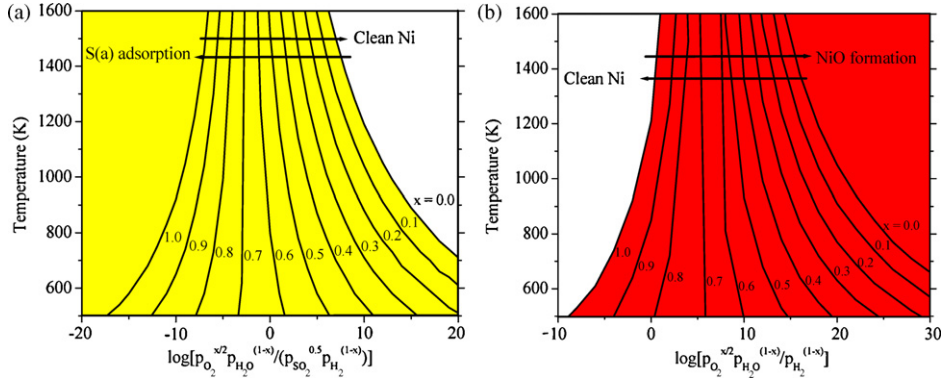


Fig. 5. The (T, p) diagrams for (a) S(a) removal and (b) NiO formation in a mixture of O_2 and H_2O of different ratio. The white, yellow, and red regions correspond to the phases of clean Ni, S(a) adsorption, and NiO bulk, respectively. The related Gibbs free energy calculations for (a) and (b) are listed in Eqs. (25) and (26), respectively. (For interpretation of the references to color in this figure legend, the reader is referred to the web version of the article.)

In addition, shown in Fig. 6(a) and (b) are the contours for the required reagent pressures to de-sulfurize the surface and to oxidize Ni, respectively, in different x values. The proper pressure ranges are in between the orders of $\log[p_{O_2}^{x/2} p_{H_2O}^{(1-x)} / p_{SO_2}^{0.5} p_{H_2}^{(1-x)}]$ for S(a) removing and $\log[p_{O_2}^{x/2} p_{H_2O}^{(1-x)} / p_{H_2}^{(1-x)}]$ for NiO formation (between the two contours). Following the analogous works in Eqs. (21) and (22), the orders of proper pressure ranges can be expressed as

$$\Delta \log \left[\frac{p_{O_2}^{x/2} p_{H_2O}^{(1-x)}}{p_{H_2}^{(1-x)}} \right] = 0.434 \left[\frac{2E_{NiO}^{DFT} - 2E_{Ni}^{DFT} - E_{SO_2}^{DFT} - E_{Ni(100)}^{DFT} - E_{S(a)}^{DFT} + H_{SO_2}}{2RT} \right] - \frac{1}{2} \log[p_{SO_2}] \quad (31)$$

The order of proper pressure range is independent of x under thermo-equilibrium conditions. It means that, in the two extreme cases, $\Delta \log[p_{O_2}^{1/2}]$ (at $x = 1$) equals to $\Delta \log[p_{H_2O}]$ (at $x = 0$), which is consistent with the results in Eqs. (21) and (22). In addition, considering the last term of $1/2 \log[p_{SO_2}]$ in Eq. (31), we can see that stronger O_2 oxidant in the reaction (23) will generate SO_2 faster and leave more residual SO_2 . Therefore, proper range for $\Delta \log[p_{O_2}^{x/2} p_{H_2O}^{(1-x)} / p_{H_2}^{(1-x)}]$ is expected to be narrower at higher x values, which is also consistent with the conclusion in Section 3.1.

It is noted that our analysis is applicable only to thermodynamic equilibrium conditions, predicting the ultimate equilibrium states under a given set of conditions (temperature and pressure). The kinetics of these reactions are important as well. However, detailed kinetic study requires additional calculations of the intermediate and transition states in the reaction paths (potential energy surface) and molecular dynamic simulations. In addition, surface morphology might change due to nickel atoms sintering or migration on the surface during the regeneration process. Further, oxygen ions transported from the cathode side may interact with the adsorbed sulfur on Ni surfaces under practical fuel cell operating conditions. These dynamic effects, which have not been taken into consideration in this study, may significantly influence the regeneration process. The methodologies to address these issues are still under investigation and will be reported in subsequent communications.

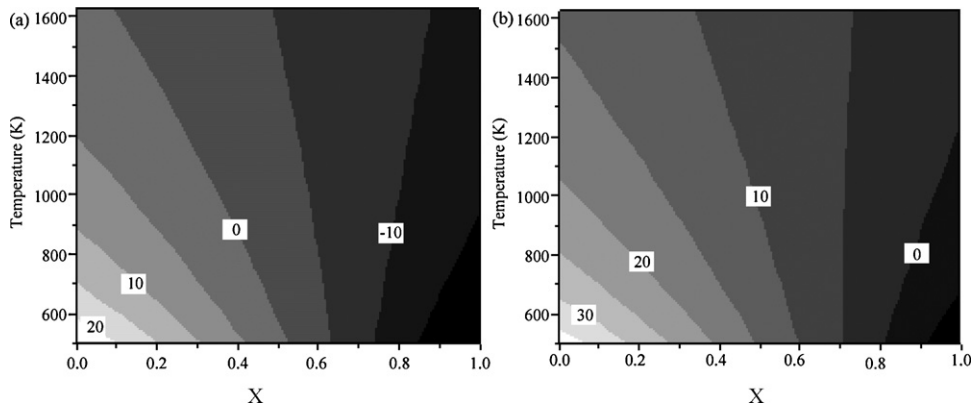


Fig. 6. Contour plots of the required pressure ratios for (a) $\log[p_{O_2}^{x/2} p_{H_2O}^{(1-x)} / p_{SO_2}^{0.5} p_{H_2}^{(1-x)}]$ in S(a) removal reaction and (b) $\log[p_{O_2}^{x/2} p_{H_2O}^{(1-x)} / p_{H_2}^{(1-x)}]$ in NiO formation.

4. Conclusion

Regeneration of sulfur-poisoned Ni surfaces by O₂, H₂O, and a mixture of them has been examined using ab initio atomistic thermodynamics. In the regeneration, both the removal of the atomically adsorbed sulfur and over-oxidation of Ni surfaces to form NiO are considered. The required temperatures and pressures of the chemical reagents needed to remove the atomic sulfur adsorbate and to form NiO are predicted and presented in thermodynamic diagrams. While both O₂ and H₂O may be used for the regeneration process, H₂O appears to be a better option because of its broader pressure range for removing surface sulfur without over-oxidizing the Ni surface.

Acknowledgements

This work was supported by the US Department of Energy (DOE) Solid State Energy Conversion Alliances (SECA) Core Technology Program (Grant No. DE-FC26-04NT42219) and DOE Office of Basic Energy Sciences, Catalysis Science Program (Grant No. DE-FG02-06ER15837) and was performed in part using the MSCF in EMSL, a national scientific user facility sponsored by the US DOE, OBER and located at PNNL. The authors also gratefully acknowledge Prof. M.C. Lin providing the computing resources in National Center for High-performance Computing in Taiwan.

References

- [1] C.H. Bartholomew, P.K. Agrawal, J.R. Katzer, *Adv. Catal.* 31 (1982) 135–242.
- [2] P.H. Holloway, J.B. Hudson, *Surf. Sci.* 33 (1972) 56–68.
- [3] D.C. Sorescu, D.S. Sholl, A.V. Cugini, *J. Phys. Chem. B* 108 (2004) 239–249.
- [4] H. Windawi, J.R. Katzer, *J. Vac. Sci. Technol.* 16 (1979) 497.
- [5] H.P. Bonzel, *Surf. Sci.* 27 (1971) 387–410.
- [6] T. Kawai, K. Kunimori, T. Kondow, T. Onishi, K. Tamaru, *J. Chem. Soc., Faraday Trans. I* 72 (1976) 833–895.
- [7] A. Travert, H. Nakamura, R.A.v. Santen, S. Cristol, J.-F. Paul, E. Payen, *J. Am. Chem. Soc.* 124 (2002) 7084–7095.
- [8] H.P. Bonzel, R. Ku, *J. Chem. Phys.* 59 (1973) 1641–1651.
- [9] A. Michaelides, P. Hu, *J. Chem. Phys.* 115 (2001) 8570–8574.
- [10] F. Dumeignil, J.-F. Paul, E. Veilly, E.W. Qian, A. Ishihara, E. Payen, T. Kabe, *Appl. Catal. A* 289 (2005) 51–58.
- [11] P. Liu, J.A. Rodriguez, T. Asakura, J. Gomes, K. Nakamura, *J. Phys. Chem. B* 109 (2005) 4575–4583.
- [12] S. Cristol, J.F. Paul, E. Payen, D. Bougeard, S. Clemendot, F. Hutschka, *J. Phys. Chem. B* 106 (2002) 5659–5667.
- [13] J.-F. Paul, E. Payen, *J. Phys. Chem. B* 107 (2003) 4057–4064.
- [14] H. He, R.J. Gorte, J.M. Vohs, *Solid State Lett.* 8 (2005) A279.
- [15] H. Kim, J.M. Vohs, R.J. Gorte, *Chem. Commun.* (2001) 2334–2337.
- [16] Y. Zeng, S. Kaytakoglu, D.P. Harrison, *Chem. Eng. Sci.* 55 (2000) 4893–4900.
- [17] T. Kanougi, T. Atoguchi, S. Yao, *J. Mol. Catal. A* 177 (2002) 289–298.
- [18] G. Liu, J.A. Rodriguez, Z. Chang, J. Hrbek, C.H.F. Peden, *J. Phys. Chem. B* 108 (2004) 2931–2938.
- [19] M. Flytzani-Stephanopoulos, M. Sakkodina, Z. Wang, *Science* 312 (2006) 1508–1510.
- [20] C.H. Bartholomew, G.D. Weatherbee, G.A. Jarvi, *J. Catal.* 60 (1979) 257–269.
- [21] A.T. Capitano, J.L. Gland, *J. Phys. Chem. B* 103 (1999) 6573–6578.
- [22] J.L. Oliphant, R.W. Fowler, R.B. Pannel, C.H. Bartholomew, *J. Catal.* 51 (1978) 229–242.
- [23] C. Lombard, S. LeDoze, E. Marenckak, P.-M. Marquaire, D. LeNoc, G. Bertrand, F. Lapique, *Int. J. Hydrogen Energy* 31 (2006) 437.
- [24] J.R. Rostrup-Nielsen, *J. Catal.* 21 (1971) 171–178.
- [25] D.R. Alfonso, A.V. Cugini, D.C. Sorescu, *Catal. Today* 99 (2005) 315–322.
- [26] Y.M. Choi, C. Compson, M.C. Lin, M. Liu, *Chem. Phys. Lett.* 421 (2006) 179–183.
- [27] D.E. Jiang, E.A. Carter, *J. Phys. Chem. B* 109 (2005) 20469–20478.
- [28] B. McAllister, P. Hu, *J. Chem. Phys.* 122 (2005) 84709.
- [29] G. Kresse, J. Furthmüller, *Phys. Rev. B* 54 (1996) 11169–11186.
- [30] G. Kresse, J. Furthmüller, *Comp. Mater. Sci.* 6 (1996) 15–50.
- [31] G. Kresse, J. Hafner, *Phys. Rev. B* 47 (1993) 558–561.
- [32] C. Lee, W. Yang, R.G. Parr, *Phys. Rev. B* 37 (1988) 785–789.
- [33] J.P. Perdew, K. Burke, M. Ernzerhof, *Phys. Rev. Lett.* 77 (1996) 3865–3868.
- [34] P.E. Blöchl, *Phys. Rev. B* 50 (1994) 17953–17979.
- [35] G. Kresse, D. Joubert, *Phys. Rev. B* 59 (1999) 1758–1775.
- [36] H.J. Monkhorst, J.D. Pack, *Phys. Rev. B* 13 (1976) 5188–5192.
- [37] J.H. Wang, M. Liu, *Electrochem. Commun.* 9 (2007) 2212–2217.
- [38] CRC Handbook of Chemistry and Physics, CRC Press, New York, 1996.
- [39] K. Reuter, M. Scheffler, *Phys. Rev. B* 65 (2001) 35406.
- [40] J. Xie, S.d. Gironcoli, S. Baroni, M. Scheffler, *Phys. Rev. B* 59 (1999) 970–974.
- [41] NIST Chemistry Webbook. <http://webbook.nist.gov/>.
- [42] W.-X. Li, C. Stampfl, M. Scheffler, *Phys. Rev. B* 68 (2003) 165412.
- [43] A. Michaelides, M.-L. Bocquet, P. Sautet, A. Alavi, D.A. King, *Chem. Phys. Lett.* 367 (2003) 344–350.